The ATLAS Electron and Photon Trigger

Samuel David Jones, on behalf of the ATLAS Collaboration [1]

School of Mathematical and Physical Sciences, Pevensey II, University of Sussex, Falmer Campus, Brighton, BN1 9QH, United Kingdom

E-mail: samuel.david.jones@cern.ch

Abstract. ATLAS electron and photon triggers covering transverse energies from 5 GeV to several TeV are essential to record signals for a wide variety of physics: from Standard Model processes to searches for new phenomena. To cope with ever-increasing luminosity and more challenging pile-up conditions in proton-proton collisions delivered by the LHC at a centre-of-mass energy of 13 TeV, the trigger selections need to be optimised to control the rates and keep efficiencies high. The ATLAS electron and photon trigger performance in Run 2 will be presented, including both the role of the ATLAS calorimeter in electron and photon identification and details of new techniques developed to maintain high performance even in high pile-up conditions.

ATL-DAQ-PROC-2018-014
12 July 2018

1. Introduction

The ATLAS [1] electron and photon (e/γ) trigger selects events with electrons and photons from the huge amount of data produced by the LHC [2]. Many interesting Standard Model processes lead to electrons and photons in the final state, for example $H \to \gamma\gamma$ in association with semileptonic top decay was a key channel for the recent observation of Higgs production in association with a top quark pair by ATLAS [3]. In addition, e/γ signatures are predicted by many new physics models, including much of the MSSM [4] parameter space.

The LHC is producing proton-proton collisions at record luminosities; the peak level of $21.4{\times}10^{33}$ cm^{-2} s^{-1} in 2018 is almost three times the peak level seen in Run 1. The centre-of-mass energy has increased from $\sqrt{s} = 7 - 8$ TeV in 2011-2012 to $\sqrt{s} = 13$ TeV in Run 2. This abundance of high energy collision data is accompanied by increased event rates and harsher pileup conditions, representing a significant challenge for triggering on e/γ signatures. Run 2 improvements to background rejection allow low trigger e/γ trigger thresholds to be maintained, whilst keeping rates at a manageable level. New developments, to be brought online in 2018, will bring the online e/γ trigger selections closer to the offline identifications, keeping efficiencies high in ever more challenging environments.

These proceedings will provide an overview of the ATLAS electron and photon triggers including recent and planned developments and e/γ trigger performance in 2016 and 2017 data taking.

2. The ATLAS Electron and Photon Triggers

Online e/γ identification at ATLAS is based on energy deposits in the calorimeter and tracking information from the Inner Detector (ID). The ID is composed of a silicon pixel detector,

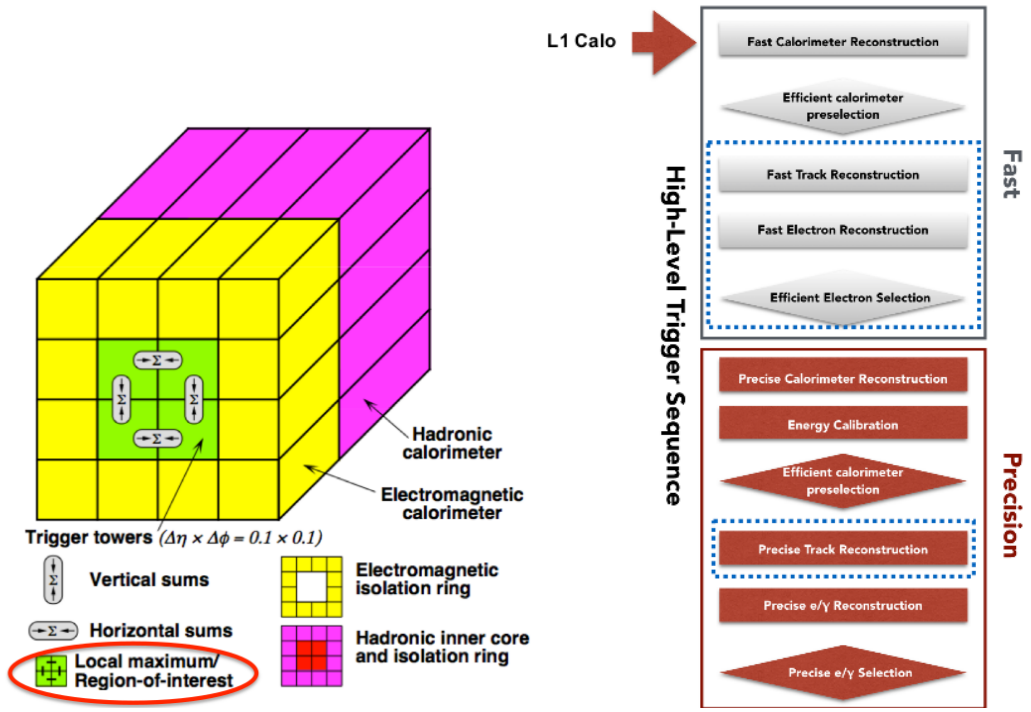

Figure 1. Schematic of the L1 calorimeter step (left) and the HLT e/γ trigger algorithm (right). Sections of the HLT trigger algorithm that apply only to electrons are surrounded by a blue dashed line. At L1 a sliding-window algorithm uses the four overlapping trigger towers highlighted in green to locate a local energy maximum for energy reconstruction. The HLT process consists of a fast sequence for early rejection which precedes more precise offline algorithms for the final selection.

a semiconductor tracker, which cover the pseudorapidity region $|\eta| < 2.5$, and a transition radiation tracker, which offers additional discrimination between electrons and hadrons in the region $|\eta| < 2.0$.

The ID is surrounded by a finely segmented calorimeter system, consisting of electromagnetic (EM) and hadronic components. A fine granularity lead/liquid argon (LAr) EM calorimeter covers the region $|\eta| < 3.2$. The hadronic calorimeter is made up of a steel/scintillator-tile calorimeter in the barrel and copper/LAr calorimeter in the endcaps, providing coverage for hadronic showers in the regions $|\eta| < 1.7$ and $1.5 < |\eta| < 3.2$, respectively.

The ATLAS trigger system uses inputs from the detector to reject events that are unlikely to yield interesting physics, reducing the event rate from 40 MHz to around 1 kHz, around 20% of which is dedicated to e/γ triggers. The trigger decision begins with the hardware-based Level 1 (L1) trigger, which identifies Regions-of-Interest (RoIs). The L1 trigger seed RoIs to the software-based High Level Trigger (HLT), which uses the full detector granularity in the RoI to provide the final trigger decision, which determines if the event is recorded for offline analysis.

The L1 e/γ trigger decision uses calorimeter information to build an RoI consisting of 4×4 trigger towers (see figure 1, left), defined as analogue summations of energy in the calorimeter cells, with granularity 0.1×0.1 in pseudorapidity (η) and azimuthal angle (ϕ). A transverse energy (E_{T}) threshold is applied, which is η dependent to account for energy losses and the geometry of the detector. A sliding-window algorithm identifies a local energy maximum using four overlapping towers within a 2×2 central region for EM energy reconstruction. The EM

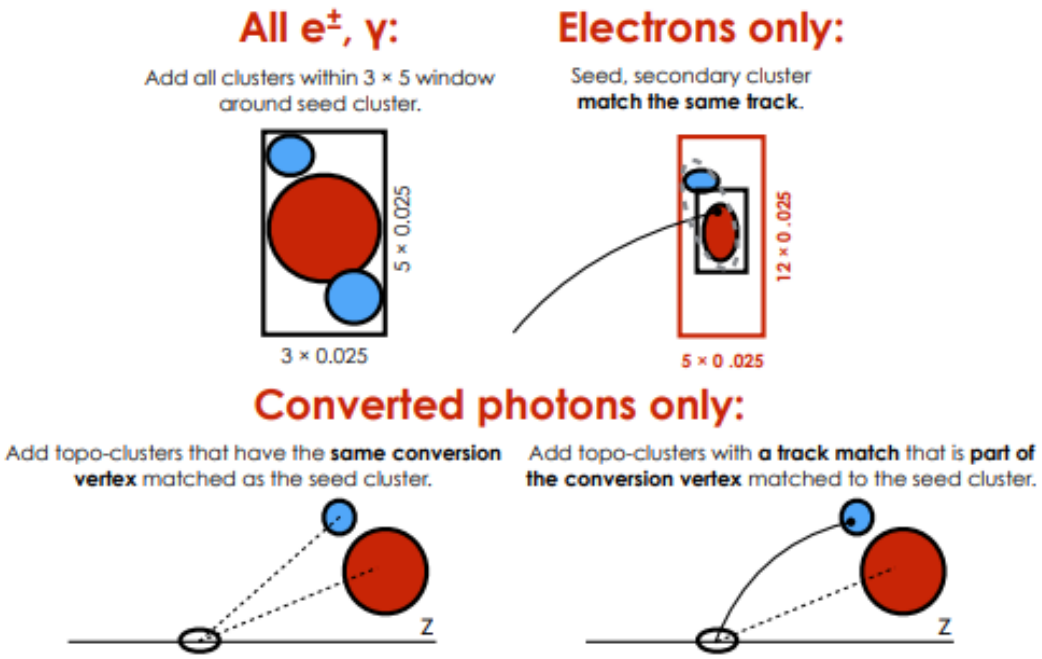

Figure 2. Diagram of the superclustering algorithm for electrons and photons.

and hadronic isolation rings are formed from the 12 towers surrounding the central cluster in the EM and hadronic layers respectively. These rings are used for isolation tests to discriminate against hadronic activity. The hadronic core energy behind the EM cluster provides additional hadronic rejection.

The e/γ algorithm sequence (see figure 1, right) proceeds in two main steps: the first step uses fast algorithms to reject events early, followed by the precision step for the efficient identification of electrons. The photon sequence follows a similar outline, without the tracking-related steps.

In the fast algorithm step, a cut-based selection is applied for photons and electrons with $E_{\mathrm{T}} < 15$ GeV, with requirements on calorimeter variables based on transverse energy and geometric energy ratios within the EM cluster. For electrons with $E_{\mathrm{T}} > 15$ GeV, the selection is based on an ensemble of neural networks, known as the *Ringer* algorithm [5]. Tracks are associated to EM clusters that pass the fast calorimeter step if they meet requirements based on $p_{\mathrm{T}}^{\mathrm{track}}$, $E_{\mathrm{T}}^{\mathrm{cluster}}$ and the track-cluster separation in pseudorapidity, $\Delta\eta(\mathrm{track}, \mathrm{cluster})$.

The precision step uses offline algorithms, with the selection is kept as close as possible to the offline selection, within CPU constraints. The offline selection, and the key differences between offline and online e/γ identification are outlined in the next section.

3. e/γ Calibration and Identification

3.1. Energy Calibration

EM cluster calibration is applied to correct for energy loss upstream of the calorimeter [6]. The calibration procedure is a simplified version of the offline calibration, applying a boosted decision tree to determine cluster energy scale factors, with separate calibrations used for electrons and photons. For the online calibration, there is no separation between converted and unconverted photons; this is one of the key differences with respect to the offline calibration.

In 2017 an alternative approach to the sliding-window algorithm (see section 1) was

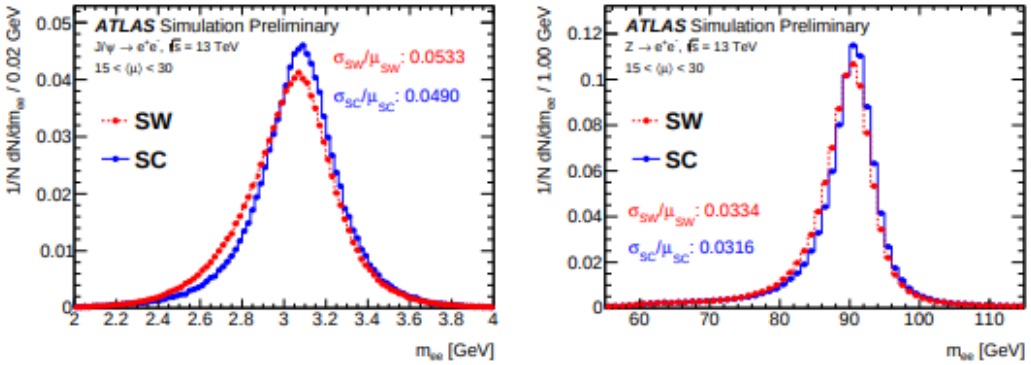

Figure 3. Invariant mass distributions from Monte Carlo simulations of $J/\psi \to e^+e^-$ decays (left) and $Z \to e^+e^-$ decays (right) for $15 < \mu < 30$, reconstructed using both sliding window and supercluster-based methods [7]. The resolution and mean for each scenario are computed using a Gaussian fit to the core of each distribution.

introduced offline, based on topological *superclusters* [7]. Superclusters are built from dynamic topological clusters, which expand outward from a seed cell in the calorimeter, identified with a high energy deposition. The topological cluster expands outwards based on the energy significance (absolute energy normalised to noise) of neighbouring cells. In this way, topological clusters match the shape of particle showers more closely than fixed size clusters.

Topological clusters allow for the reconstruction of low energy showers of $\mathcal{O}(100)$ MeV. Thus photons emitted from bremsstrahlung interactions in the ID can be recovered and matched to their associated electron, forming a supercluster. The formation of superclusters is based on spatial separation, with additional track matching for electrons (see figure 2).

The recovery of energy lost due to bremsstrahlung leads to a 30-40% improvement in energy resolution, with the largest improvements at low transverse energy. This improvement translates to a 5-10% improvement in offline mass resolution (see figure 3), with similar improvements expected online. This approach is planned to be introduced for online e/γ identification in 2018.

3.2. Identification

A common set of calorimetric variables is used for electron and photon identification [8][9]. These variables are based on properties of the EM cluster such as the shower shape and energy ratios between cells within the cluster. In Run 1, cut-based identification selections were used online and by default offline for both electrons and photons. The cut-based photon selection was reoptimised for harsher pileup conditions, and higher instantaneous luminosity and centre-of-mass energy in Run2. For electron identification in Run 2, a likelihood (LH) based approach was introduced for offline electron identification. The LH method is a multivariate analysis technique, simultaneously evaluating electron cluster, track and track-cluster matching variables to form a LH discriminant:

$$d_{\mathcal{L}} = \frac{\mathcal{L}_S}{\mathcal{L}_S + \mathcal{L}_B}, \qquad \mathcal{L}_{S(B)}(\vec{x}) = \prod_{i=1}^{n} P_{s(b),i}(x_i) \tag{1}$$

where $\mathcal{L}_{S(B)}$ is the signal (background) likelihood, $\vec{x}$ is a vector of the input variables and $P_{s(b),i}(x_i)$ are the signal (background) probability densities corresponding to each of the inputs. Three ID levels are formed by cutting on different values of the LH discriminant $d_{\mathcal{L}}$. These

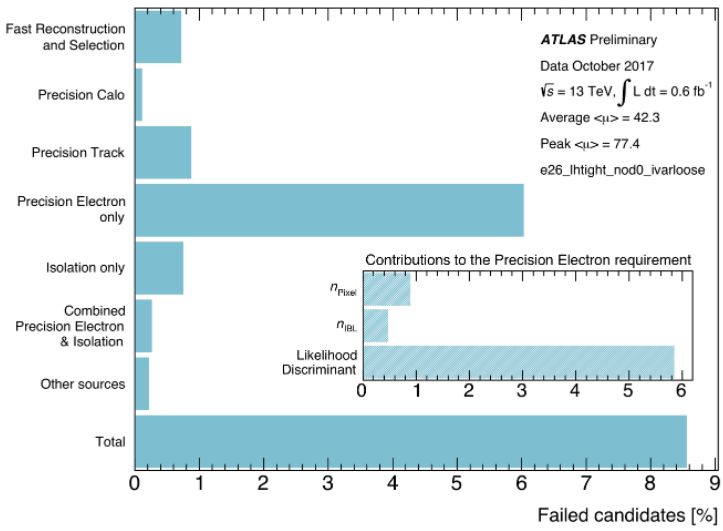

Figure 4. Sources of inefficiency for an electron trigger with threshold 26 GeV, tight LH identification and isolation requirements, at each selection step in the High Level Trigger (HLT) with respect to the offline reconstruction and the corresponding Level-1 (L1) requirements in a data run taken in October 2017 [12].

represent a tradeoff between purity and efficiency and are chosen such that the samples of electrons selected are subsets of looser IDs.

The LH applied for online electron identification is kept as close as possible to offline, with some differences due to online reconstruction constraints, for example no transverse track impact parameter cut is applied and the track momentum resolution is not used. Instead of using the energy-momentum ratio at high transverse energy, a looser trigger is applied to recover efficiency in this regime, and the average pileup per bunch crossing is used instead of the number of vertices in the event. The online version of the LH achieves a 20% rate reduction compared to a cut-based selection of a similar efficiency, and is the default for Run 2.

3.3. Tracking at HLT

Precision tracking contributes significantly to inefficiency at HLT, measured with respect to offline identification with L1 requirements applied (see figure 4). Track trajectories are currently fitted online using the linear Kalman Filter [10] at HLT. This is in contrast to offline fitting, where a nonlinear generalisation of the Kalman filter is used, the so called Gaussian Sum Filter (GSF) [11]. The GSF approximates the experimental noise as a weighted sum of Gaussian functions, applying a Kalman filter on each Gaussian component. The nonlinear GSF approach can be more suitable for the tracking of electrons, where radiative losses can be substantial, altering the track. Compared with standard tracking, GSF improves offline electron reconstruction efficiency in most η regions of the detector by up to 6%. GSF tracking will be introduced online at ATLAS in 2018. This will allow for closer alignment of the online and offline selections, with similar improvements expected online due to improved resolution in tracking variables.

4. e/γ Trigger Performance in 2016 and 2017

The electron trigger output rate displays a nonlinear dependence on the transverse energy threshold (see figure 5). It is dominated by $W \to e\nu$ events (around 55%), with subdominant contributions from multijet (35%) and $Z \to ee$ (10%). By applying a threshold greater than

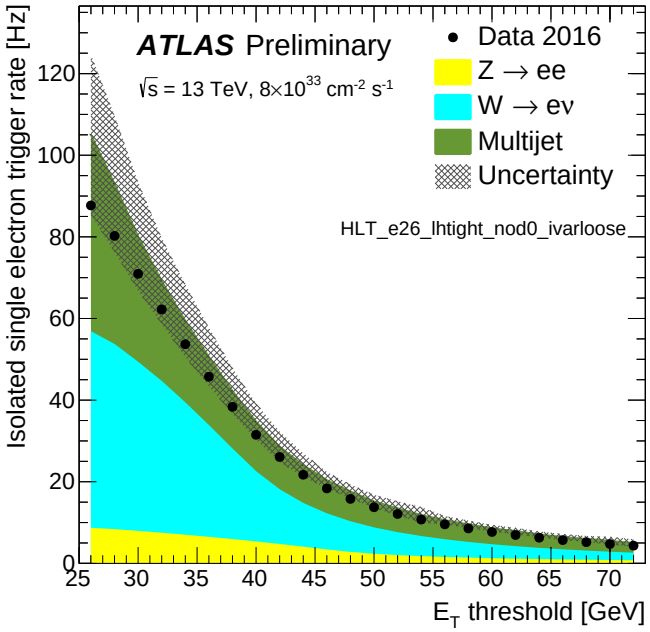

Figure 5. Rate (in Hz) of the isolated single electron trigger as a function of the ET threshold at the high-level trigger (HLT) in the [26,72] GeV range, for the same likelihood-based tight identification and Level-1 selections [12].

$M_W/2$ the electron trigger rate can be significantly reduced. The rate also depends linearly on the instantaneous luminosity for electron and photon triggers (see figure 6). As the instantaneous luminosity increases, the rates are managed by tightening the transverse energy threshold and the selection. For example, by moving from the *medium* to the *tight* likelihood working point, a rate reduction of 45% was achieved.

Electron isolation requirements provide further discrimination against non-prompt electrons and photons originating from hadronic activity. For electrons, variable track isolation is applied at HLT, placing an upper cut on the p_{T} sum of non-electron associated tracks in a cone with size given by the ratio 10 GeV / p_{T} surrounding the electron candidate, with a maximum cone size of 0.2. Calorimetric isolation, using the transverse energy sum of topological clusters in a cone surrounding the photon candidate, was introduced for online photons in 2017. Trigger isolation gives a rate reduction of around 10% for the primary electron trigger at threshold 26 GeV, and around $20-40$% for diphoton triggers at threshold 22 GeV, depending on the isolation working point used.

At high transverse energies, track isolation losses become important for electrons. To mitigate the efficiency loss in this regime, a logical OR is used with higher threshold, looser identification and no isolation requirements. The effect can be seen in the overall efficiency vs. transverse energy in figure 7 at 60 GeV where a discontinuity is seen in the trigger turn-on. A significant increase in efficiency in the plateau is achieved with minimal contribution to the electron trigger rate.

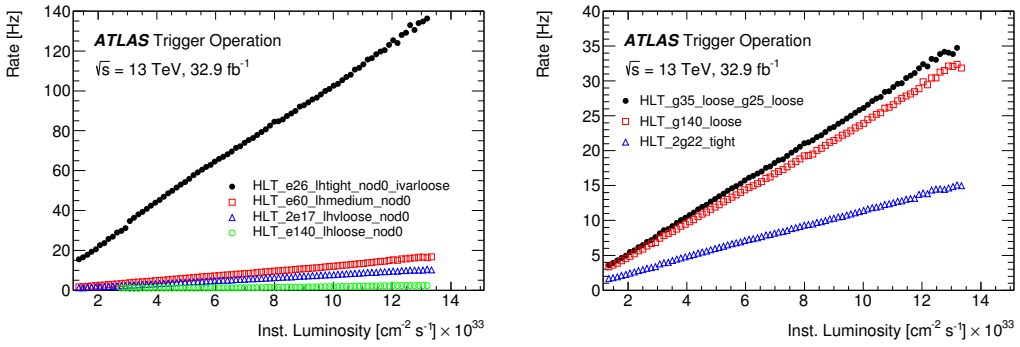

Figure 6. Output rates of primary electron electron (left) and photon (right) triggers as a function of the uncalibrated instantaneous luminosity during 2016 data taking [12].

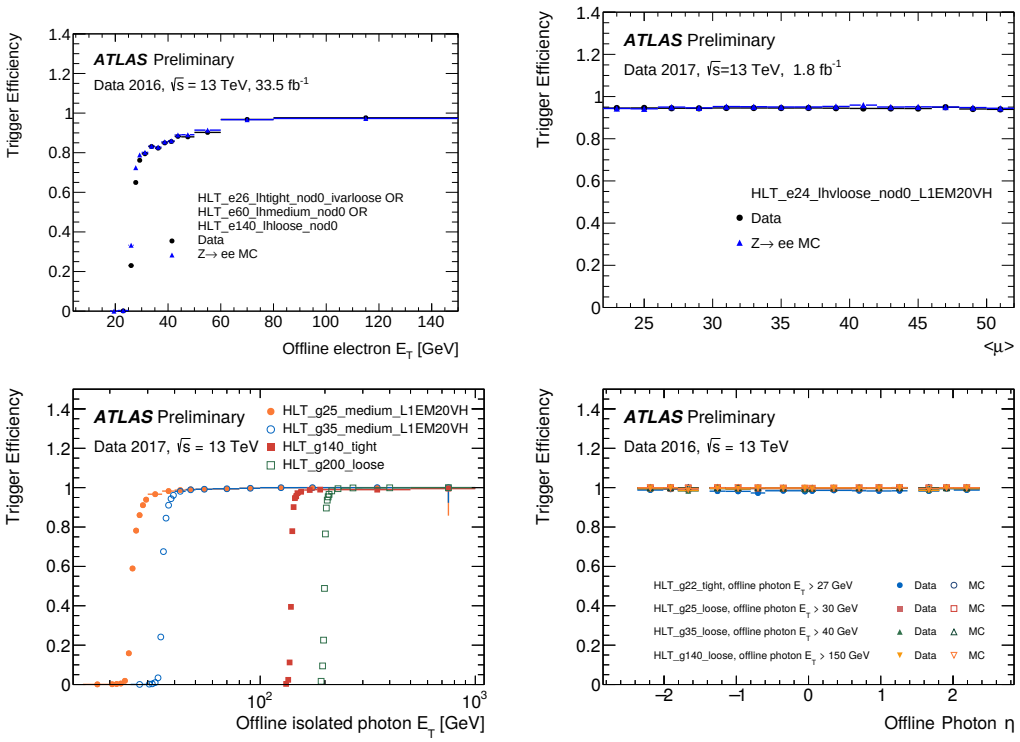

Figure 7. Electron (top) and photon (bottom) trigger efficiencies in 2016 and 2017 [12]. The efficiencies are shown as a function of transverse energy (left) and pseudorapidity (right). The electron efficiency is measured using the *Tag and Probe Method* using $Z \rightarrow ee$ decays for data and Monte Carlo. The photon efficiency is measured with the *bootstrap* method using events recorded with a looser Level 1 trigger.The naming convention is as follows: *HLT* indicates a High Level Trigger, *e (g)* indicates an electron (photon) trigger, the subsequent number indicates the transverse energy threshold, next the identification level is identified (*tight, loose* or *medium*), where *lh* is used to indicate a likelihood based trigger. *nod0* indicates that no transverse impact parameter cuts are required and *ivarloose* indicates a variable sized cone isolation requirement.

5. Conclusions

Physics signatures with electrons and photons form an essential part of the ATLAS physics program. Ever increasing instantaneous luminosity and pileup present significant challenges for data collection. Improvements to background rejection, for example the LH discriminant and isolation requirements, have allowed low thresholds to be maintained. The online e/γ trigger selections are kept as close as possible to offline identification to keep performance optimal and the ATLAS electron and photon triggers have operated at high efficiency throughout Run 2. Planned improvements for 2018, for example GSF tracking and superclustering, will bring the online selection even closer to offline. With the LHC running at design luminosity in 2018, more than 100 fb^{-1} of collision data will be collected by ATLAS by the end of Run 2. With the ATLAS e/γ triggers continuing to perform well, this is an exciting prospect for physics in electron and photon signatures.

References

[1] ATLAS Collaboration 2008 *JINST* **3** S08003

[2] Evans L and Bryant P 2008 *JINST* **3** S08001

[3] ATLAS Collaboration 2018 `arXiv:1806.00425` [hep-ex]

[4] Csaba Csáki 1996 `arXiv:9606414v1` [hep-ph]

[5] João Victor da Fonseca Pinto 2016 J. Phys.: Conf. Ser. 762 012049

[6] ATLAS Collaboration 2016 ATL-PHYS-PUB-2016-015 https://cds.cern.ch/record/2203514/

[7] ATLAS Collaboration 2017 ATL-PHYS-PUB-2017-022 https://cds.cern.ch/record/2298955

[8] ATLAS Collaboration 2016 ATLAS-CONF-2016-024 https://cds.cern.ch/record/2157687

[9] ATLAS Collaboration 2012 ATLAS-CONF-2012-123 https://cds.cern.ch/record/1473426

[10] R. Fruehwirth 1987 Nucl. Instrum. Meth. **A262** 444

[11] ATLAS Collaboration 2012 ATLAS-CONF-2012-047 https://cds.cern.ch/record/1449796

[12] ATLAS Collaboration Public Egamma Trigger Plots for Collision Data `https://twiki.cern.ch/twiki/bin/view/AtlasPublic/EgammaTriggerPublicResults`